Applied Catalysis B: Environmental 188 (2016) 23–30

Contents lists available at ScienceDirect

Applied Catalysis B: Environmental

journal homepage: www.elsevier.com/locate/apcatb

Synthesis and characterization of a novel tungstosilicic acid immobilized on zeolites catalyst for the photodegradation of methyl orange

Candelaria Leal Marchena[a,c,1], Laura Lerici[a,c], Soledad Renzini[a,c], Liliana Pierella[a,c], Luis Pizzio[b,c,*]

[a] Centro de Investigación y Tecnología Química (CITeQ), UTN—CONICET, Maestro Marcelo Lopez y Cruz Roja Argentina, 5016 Córdoba, Argentina
[b] Centro de Investigación y Desarrollo en Ciencias Aplicadas "Dr. J.J. Ronco" (CINDECA), Departamento de Química, Facultad de Ciencias Exactas, UNLP-CCT La Plata, CONICET, 47 No. 257, 1900 La Plata, Argentina
[c] Conicet (Consejo Nacional de Investigaciones Científicas y Técnicas), Argentina

ARTICLE INFO

Article history:
Received 4 August 2015
Received in revised form
18 December 2015
Accepted 26 January 2016
Available online 29 January 2016

Keywords:
Photocatalysis
Zeolites
Tungstosilicic acid
Azoic dye

ABSTRACT

Materials based on tungstosilicic acid (TSA) immobilized on zeolites (NH_4Y and NH_4ZSM5) were prepared by wet impregnation of the zeolite matrix with TSA aqueous solutions. The concentration was varied in order to obtain TSA contents of 5%, 10%, 20%, and 30% w/w in the solid. Catalysts were further characterized by N_2 adsorption–desorption isotherms, FT-IR, XRD, DRS-UV–vis and SEM techniques. The resulting materials were evaluated in the photodecomposition of azo dye methyl orange. The results revealed that the materials present suitable properties to be used as catalysts in the photocatalytic treatment of wastewater containing dyes, and the photodegradation follows a pseudo-first-order kinetics. Reaction parameters such as TSA content, catalysts mass, reuses and pH, were evaluated.

© 2016 Published by Elsevier B.V.

1. Introduction

Wastewaters resulting from human activities can contain many organic and inorganic substances and they are one of the main sources of environmental pollution due to the fast industrial development. Anthraquinone, arylmethane, indigoid and azo dyes, used on a large scale particularly in textile industries, may generate toxic substances through oxidation, hydrolysis or other chemical reactions occurring in the wastewater phase [1]. For this reason, the development of procedures to control or destroy this type of pollution is of great interest and a challenge.

Up to the present time, different methods have been developed for removing colored pollutants from wastewaters. The most common methods are coagulation/flocculation and removal by activated carbon [2–4] which generates huge amounts of sludge and waste that should be disposed. A new and effective approach for the removal and degradation of dyes are the advanced oxidation processes (AOPs). Among the different AOPs, the photoassisted catalytic decomposition of organic pollutants employing semiconductors as photocatalysts is promising [5,6].

Methyl orange is an azo dye that has been widely used as a model compound for the research on photoreactions [7,8]. Many researchers have reported the decomposition of methyl orange using TiO_2 as a photocatalyst under ultraviolet irradiation or solar irradiation [9–12].

Heteropolyacids with Keggin structure have received increasing attention in many research applications, such as acid catalysts and redox [13–15]. Currently, heteropolyacids are used as photocatalysts for the degradation of organic pollutants in water due to their nontoxicity and photostability [16–18]. Tungstophosphoric acid ($H_3PW_{12}O_{40}$, TPA) is one of the most studied and used heteropolyacids due to its high Brönsted acidity, high thermal stability and low reducibility, among other qualities [19–21]; tungstosilicic acid ($H_4SiW_{12}O_{40}$, TSA) shows similar and comparable characteristics, but is less taken into account.

Heteropolyacids have photocatalytic properties comparable to the best-known semiconductors such as TiO_2, ZnO, CdS, etc. [22,23].

* Corresponding author at: Centro de Investigación y Desarrollo en Ciencias Aplicadas "Dr. J.J. Ronco" (CINDECA), Departamento de Química, Facultad de Ciencias Exactas, UNLP-CCT La Plata, CONICET, 47 No. 257, 1900 La Plata, Argentina.
E-mail addresses: cleal@frc.utn.edu.ar (C. Leal Marchena), lrpizzio@quimica.unlp.edu.ar (L. Pizzio).
[1] Co-corresponding author.

http://dx.doi.org/10.1016/j.apcatb.2016.01.064
0926-3373/© 2016 Published by Elsevier B.V.

Both TPA and TSA absorb in the region of visible and near UV, generating a charge-transfer excited state of the isolated metal oxospecies $[Me^{(n-1)+}\text{-}O^{\bullet}]^*$ formed. The difference between TPA and TSA lies primarily in the charge difference in the heteropolyanion. Choi et al. [24] evaluated the redox behavior and catalytic properties of Keggin-type heteropolyacids (Co^{2+}, B^{3+}, Si^{4+} and P^{5+}) in the oxidation of benzaldehyde and determined the potential reduction, which was correlated with the heteropolyanion charge. It was also reported that the charge difference generates different interactions between the heteropolyacids and the solid surfaces. Pruethiarenun et al. [25] synthesized and compared brookite hybrid films with TPA and TSA, demonstrating that the higher charge of $[SiW_{12}O_{40}]^{4-}$ with respect to $[PW_{12}O_{40}]^{3-}$ results in lower interaction with the material.

The main drawback of polyoxometalates as catalysts is their low surface area (lower than 10 m^2/g) and high solubility in polar organic solvents and water, which makes it impossible to recover and reuse these materials [26,27]. Such problem could be overcome by supporting them on suitable porous materials with high surface area to obtain a greater number of available and accessible acidic sites. The high surface area could result in a high concentration of active catalytic sites. Moreover, the supported heteropolyacids are more thermally stable than ion exchange resins and they are practically insoluble [28]. It was reported that polyoxometalate salts were combined and supported on photoactive and/or inactive materials seeking to improve their properties [29–31]. Supporting the polyoxometalates on solid surfaces, such as zeolites, activated carbon, SiO_2, Al_2O_3, among others [32]. increases their specific surface area and allows an easy recovery and reuse of hybrid catalysts.

Zeolites are microporous crystalline aluminosilicates with structural characteristics, such as the ability to trigger photoinduced electron donor and acceptor reactions, which makes them attractive hosts for photochemical applications [33,34]. The application of zeolites as supports provides photospecific properties such as the control of charge-transfer and electron-transfer processes, causing an increase in the photoactivity of the catalysts obtained [35,36]. This increase has been attributed, among other factors, to the stabilizing effect on the redox species photogenerated, and control over charge-transfer and electron-transfer processes [36–38]. The stabilization of the charge-transfer state of many reactions and transient species, such as $^{\bullet}OH$ and $^{\bullet}O^{2-}$ in the presence of zeolites, has also been reported in several studies [39–46]. Additionally, the acidity of zeolite plays a crucial role on the Keggin anion stability, because it is strongly related with the acidity of the support. For example, when NH_4Y and NH_4ZSM5 zeolites were used as supports for tungstophosporic acid (TPA), the Keggin structure was more stable on ZSM-5 and it was attributed to its higher acidity [47]. When Al_2O_3 was evaluated as support for TPA, the Keggin anion was partially transformed into the $[P_2W_{21}O_{71}]^{6-}$ specie [32].

Chen et al. [48] employed HZSM5 zeolite with a Si/Al ratio of 14.2 for in situ synthesis and impregnation of $H_3PMo_{12}O_{40}$, obtaining an improvement in the *n*-octane hydroconversion. Pamin et al. [29] found that TPA was stabilized when it was supported in lower Si/Al ratio (2.47) zeolite Y. We reported [47] that both NH_4Y (Si/Al = 2.47) and NH_4ZSM-5 (Si/Al = 17) zeolites were suitable for TPA immobilization. Even when a huge number of ordered porous materials and amorphous silicoaluminates could be employed as supports for the heteropolyacids, zeolites were selected based on the before mentioned studies.

In the present work we attempted to combine the well-known but not deeply investigated photocatalytic properties of TSA and the above-mentioned properties of zeolites as heteropolyacid supports in order to synthesize heterogeneous photocatalytic materials. The resulting materials were evaluated in the photodecomposition of azoic dye methyl orange. We also analyzed a kinetic study of the degradation of methyl orange employing a new material for this process (TSA-Zeolite) as heterogeneous photocatalytic materials with the objective of applying the photoreaction to water cleanup technology.

2. Experimental

2.1. Catalyst preparation

The zeolite NH_4Y (Si/Al = 2.47) was provided by Aldrich. ZSM-5 material (Si/Al = 17) was obtained by the hydrothermal crystallization method [49] with some modifications made by our group. Aqueous solution of sodium aluminate ($NaAlO_2$, Johnson Matthey Electronics) was added to a silica anhydride (Fluka) solution that was previously prepared by partial dissolution of tetrapropylammonium hydroxide (TPAOH, Fluka) in water. The obtained gel reached a pH > 9 and was maintained at 120–160 °C for 12–16 days under self-generated pressure on autoclave. Afterwards, the reaction products were extracted, washed and dried at 100 °C for 12 h. The structure directing agent (TPAOH) was desorbed in N_2 atmosphere (20 ml/min) at programmed temperature (10 °C/min) from 25 to 500 °C and then it was calcined in air at 500 °C for 12 h to obtain Na-ZSM5. The ammonium form of the material (NH_4ZSM5) was prepared by ion exchange with NH_4Cl (1 M) for 40 h at 80 °C from Na-zeolite.

The TSA solutions were prepared from tungstosilicic acid ($H_4SiW_{12}O_{40}.23H_2O$, Fluka p.a.) and using distilled water as solvent. TSA was incorporated into the zeolite matrix by wet impregnation in a rotary evaporator at 80 °C. The solids were calcined in air at 200 °C for 2 h. The amount of TSA deposited onto the surface of the zeolites was varied with the purpose of obtaining a TSA concentration of 5%, 10%, 20% and 30% by weight in the final solids, named $TSA05NH_4Y$, $TSA10NH_4Y$, $TSA20NH_4Y$, and $TSA30NH_4Y$, respectively; and for zeolite NH_4ZSM5, $TSA05NH_4ZSM5$, $TSA10NH_4ZSM5$, $TSA20NH_4ZSM5$ and $TSA30NH_4ZSM5$, respectively.

For comparative purposes, the ammonium salt of tungstosilicic acid $[(NH_4)_4SiW_{12}O_{40}]$ was synthesized following a previously reported procedure [50]. An aqueous solution of NH_4Cl [0.073 mol/l] was added dropwise to ca. 50 ml of a 50/50 ethanol/water solution of $H_4SiW_{12}O_{40}$ [0.025 mol/l] under vigorous stirring to form a white colloidal solution, which contains well-dispersed $(NH_4)_4[SiW_{12}O_{40}]$ precipitates. The rate addition was ca. 0.4 ml/min, and the time taken for the addition of NH_4Cl was ca. 150 min. During the procedure, the $H_4SiW_{12}O_{40}$ solution was kept at a constant temperature of 25 °C. The resulted solution was aged for 30 min at the same temperature. Then, it was dried at 55 °C with a vacuum rotary evaporator to obtain the white powder of $(NH_4)_4[SiW_{12}O_{40}]$.

2.2. Sample characterization

The specific surface area and the mean pore diameter of the solids were determined from the N_2 adsorption–desorption isotherms at the liquid-nitrogen temperature, obtained using Micromeritics PulseChemisorb 2700 equipment. The solids were previously degassed at 100 °C for 2 h.

The Fourier transform-infrared (FT-IR) spectra of the solids were obtained using a JASCO 5300 spectrometer and pellets in KBr in the 400–4000 cm^{-1} wavenumber range.

The X-ray diffraction (XRD) patterns were recorded with Philips PW-3020 equipment with a built-in recorder, using CuKα radiation, nickel filter, 20 mA and 40 kV in the high voltage source, and scanning angle between 5 and 50° 2θ at a scanning rate of 2° per minute.

The diffuse reflectance spectra (DRS-UV–vis) of the materials were recorded using a UV–vis JASCO V 650 spectrophotometer, to which a diffuse reflectance chamber with an integrating sphere of 50 mm diameter and internal Spectralon coating is attached, in the 200–800 nm wavelength range. From DRS-UV–vis spectra the band gap energy (Eg) of the materials was estimated using Kubelka-Munk remission function [51].

The morphological characteristics of supported catalysts were determined by scanning electron microscopy (SEM) in a Philips Model 505 microscope at 14–20 Kv accelerating voltage using fine catalyst powder supported on carbon tape over an aluminum tip and coated with gold.

2.3. Photocatalytic experiments

Methyl orange (MO), used as a model contaminant, is an azo dye that exhibits acid-base equilibrium in solution with $pK_a = 3.5$. Under neutral conditions, MO exists as negative charged form with orange color ($\lambda_{max} = 464$ nm, $\varepsilon = 24600$). The band at 464 nm that is associated with the azo bond (—N=N—) was used to monitor the effect of photocatalysis on the degradation of MO under neutral conditions. Rochkind et al. [52] advised that dyes are inappropriate as model compounds for the evaluation of photocatalytic activity of novel photocatalysts claimed to operate under visible light. So, the performances of our materials were measured using a high-pressure mercury lamp with a maximum emission in the UV region.

The photocatalytic degradation of methyl orange (MO) was performed in a cylindrical Pyrex glass photochemical reactor thermostated by water circulation in order to maintain the temperature at 25 °C. The tests were carried out employing a 125 W high-pressure mercury lamp (with a maximum emission at 365 nm and the light intensity at about 20 mW/cm^2) placed inside a Pyrex glass jacket thermostated by water circulation and immersed in the MO solution. The catalyst was maintained in suspension by stirring and air was continuously bubbled at a flow of 0.9 l/min. Previously, the MO solution (400 ml, $C^0_{MO} = 8 \times 10^{-5}$ mol/l) containing 200 mg of catalyst was magnetically stirred in the absence of light for 30 min to ensure the adsorption–desorption equilibrium of MO on the surface of the materials. During the course of the experiments, samples were periodically withdrawn, filtered using a Millipore syringe adapter (porosity, 0.45 μm) and then analyzed. The variation of the MO concentration as a function of the reaction time was measured spectrophotometrically using a Jasco 7800 double-beam UV–vis spectrophotometer. The concentration change was calculated from the linear calibration plot of MO at a wavelength of 464 nm.

3. Results and discussion

3.1. Catalyst characterization

The specific surface area (S_{BET}) of the synthesized materials, zeolites (NH_4Y, NH_4ZSM5), TSA and its ammonium salt $(NH_4)_4[SiW_{12}O_{40}]$, determined from N_2 adsorption–desorption isotherms using Brunauer–Emmett–Teller (BET) method, is listed in Table 1. According to IUPAC classification, the N_2 adsorption–desorption isotherms of NH_4Y and NH_4ZSM5 zeolites can be classified as Type I, characteristic of microporous solids having relatively small external surfaces. The N_2 adsorption–desorption isotherms of the $TSANH_4Y$ and $TSANH_4ZSM5$ samples exhibit similar characteristics to that of the respective zeolite. The S_{BET} values decrease with the increment of TSA content in the sample. Taking into account that the pore diameter of NH_4Y and NH_4ZSM5 are 0.74 nm and 0.56 nm, respectively [53]. the progressive decrease in S_{BET} could be due to the clogging of zeolite pores by the $[SiW_{12}O_{40}]^{4-}$ anions, which have a diameter of 1.2 nm.

Table 1
Specific surface area, crystallite size and optical band gap of zeolite, TSA and the impregnated materials.

Samples	S_{BET} (m^2/g)	D_C (nm)[a]	E_g (eV)
TSA	9	0.4	2.80
$(NH_4)_4[SiW_{12}O_{40}]$	101	0.4	2.90
NH_4Y	485	1.0	5.05
$TSA05NH_4Y$	446	1.0	3.11
$TSA10NH_4Y$	410	0.9	3.00
$TSA20NH_4Y$	376	1.0	2.95
$TSA30NH_4Y$	362	1.0	2.95
NH_4ZSM5	355	0.4	5.70
$TSA05NH_4ZSM5$	340	0.4	3.12
$TSA10NH_4ZSM5$	329	0.4	3.12
$TSA20NH_4ZSM5$	312	0.4	3.10
$TSA30NH_4ZSM5$	286	0.4	3.08

[a] D_C values were calculated using the (1, 1, 1) and (1, 0, 1) crystal plane corresponding to NH_4Y and NH_4ZSM5 samples, respectively.

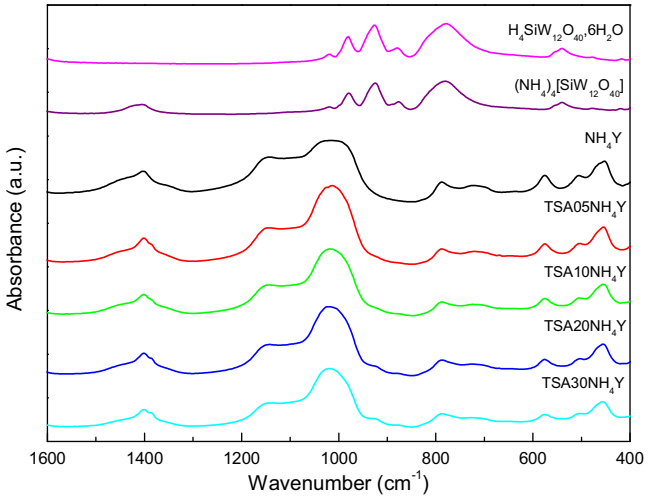

Fig. 1. FT-IR spectra of $H_4SiW_{12}O_{40}$, $(NH_4)_4[SiW_{12}O_{40}]$, NH_4Y and $TSANH_4Y$ samples.

The FT-IR spectrum of NH_4Y (Fig. 1) shows the bands between 1250 and 950 cm^{-1} that are assigned to asymmetrical stretching vibrations corresponding to the tetrahedral Si, Al atoms of the structures. The bands at 790 and 720 cm^{-1} are assigned to Si—O symmetrical stretching vibrations. The presence of structural double six-membered rings in the case of NH_4Y zeolite originates the band at 550–555 cm^{-1}. The FT-IR spectrum of NH_4ZSM5 zeolite exhibits the bands between 1250 and 950 cm^{-1} (assigned to asymmetrical stretching vibrations), the band at 800 cm^{-1} (Si—O symmetrical stretching vibrations) and at 550–555 cm^{-1} (structural double five-membered rings). The band appearing between 465 and 455 cm^{-1} in both matrices can be assigned to the structure-insensitive internal tetrahedral bending bond, i.e., T–O_4 (T: Si or Al) [53].

In the TSA spectrum, the bands were observed at 1019, 982, 926, 884, 782, and 540 cm^{-1}, which agrees with those referred to in the literature [54]. The first band is not assigned, while the others correspond to the stretching vibrations W—O_d, Si—O_a, W—O_b—W and W—O_c—W and to the bending vibrations O_a—Si—O_a + W—O—W, respectively. The subscripts indicate oxygen bridging the W and the heteroatom (a) corner-sharing oxygen, (b) edge-sharing oxygen, (c) belonging to WO_6 octahedral, and (d) terminal oxygen.

The spectrum of the salt $(NH_4)_4[SiW_{12}O_{40}]$, as well as the bands assigned to the Keggin anion, presents a band at 1415 cm^{-1} attributed to the N—H stretch. The spectra of the samples

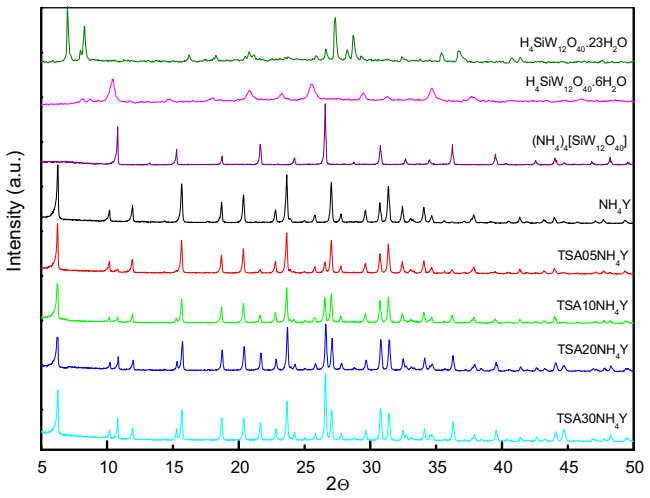

Fig. 2. XRD patterns of $H_4SiW_{12}O_{40}.23H_2O$, $H_4SiW_{12}O_{40}$, $(NH_4)_4[SiW_{12}O_{40}]$, NH_4Y, $TSA05NH_4Y$, $TSA10NH_4Y$, $TSA20NH_4Y$ and $TSA30NH_4Y$ samples.

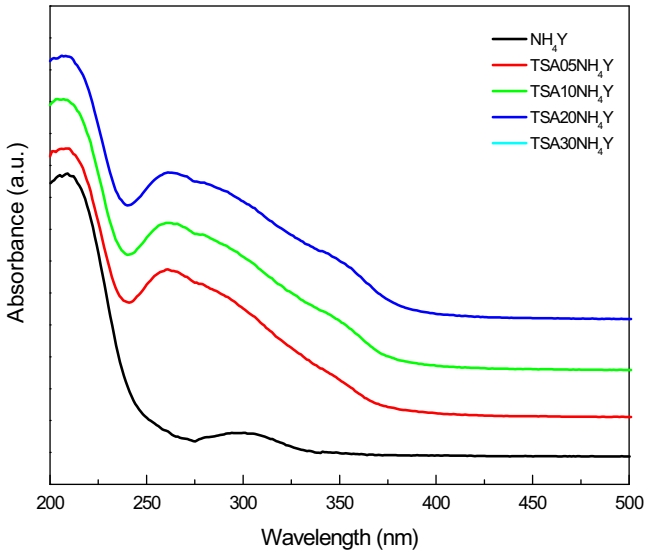

Fig. 3. DRS-UV–vis spectra of the NH_4Y, $TSA05NH_4Y$, $TSA10NH_4Y$, $TSA20NH_4Y$ and $TSA30NH_4Y$ samples.

$TSA05NH_4Y$, $TSA10NH_4Y$, $TSA20NH_4Y$ and $TSA30NH_4Y$ show, overlying the zeolite, characteristic bands overlapped with those of TSA, whose relative intensity increases with the increment of TSA content. The spectrum of the $TSANH_4ZSM5$ samples shows an increase in the signals 982, 926 and 884 cm^{-1}, assigned to the heteropolyacid with the increased amount of TSA. Additionally, in both cases, the band of zeolite at 782 cm^{-1}, assigned to the vibrations related to external linkages between tetrahedra and sensitive to the framework structure, gets wider as a result of its superposition with the W–O_c–W stretching of TSA [55].

The XRD pattern (Fig. 2) of $H_4SiW_{12}O_{40}.6H_2O$ shows the characteristic peaks at $2\theta = 10.5$, 26 and 30°, corresponding to the [110], [222], and [400] planes, in agreement with the literature [56].

The XRD patterns of the $TSANH_4Y$ and $TSANH_4ZSM5$ samples show the presence of the characteristic peaks of zeolite NH_4Y and NH_4ZSM5 respectively, but with lower intensity. The XRD diffraction patterns also have an additional set of peaks, which are different from those presented by $H_4SiW_{12}O_{40}$, its hydrate, $H_4SiW_{12}O_{40}.23H_2O$, or other crystalline phases resulting from the processing [57]. These peaks are similar to those of salt $(NH_4)_4[SiW_{12}O_{40}]$, whose formation is due to the interaction of the anions $[SiW_{12}O_{40}]^{4-}$ with the $[NH_4]^+$ present in both zeolites.

It has been reported [58] that the interaction between $H_3PW_{12}O_{40}$ and supports such as SiO_2, TiO_2 or ZrO_2 can be assumed to be of the electrostatic type due to the transfer of protons to M-OH according to:

$$M\text{-}OH + H_3PW_{12}O_{40} \rightarrow [M\text{-}OH_2^+][H_2PW_{12}O_{40}^-]$$

The proton transfer from $H_3PW_{12}O_{40}$ to the amine group, resulting in an electrostatic bond between $-NH_3^+$ and $[H_{3-x}PW_{12}O_{40}]^{x-}$ (where $1 < x \leq 3$), is responsible for the efficient immobilization of the heteropolyanion [59,60].

The crystallite size (D_C) (Table 1) of the new crystalline phase, estimated by XRD patterns using Scherrer's equation, seems to be independent of the TSA contents in the samples ($TSANH_4Y$ and $TSANH_4ZSM5$) and similar to those of zeolite. In general, an increase of supported species causes an increase in the crystal size, but this effect does not occur in these samples, probably due to the good distribution achieved on the surface of TSA.

The charge-transfer absorption spectra of most nonreduced heteropolyanions obtained by DRS-UV–vis appear in the 200–500 nm region and consist of bands that may be ascribed to oxygen-to-metal transfers. The bulk TSA spectrum presents two broad bands that extend from 250 to 450 nm, assigned to the charge transfer from bridging or terminal O 2p to W 5d (W-O-W and W-O_d, respectively) [32,61].

The DRS-UV–vis spectrum (Fig. 3) of NH_4Y consists of two bands at 216 nm and 300 nm, the first one due to the Al-O charge transfer transition of four–coordinated framework aluminum, and the second one attributed to structures with highly ordered octahedral symmetry [62]. For NH_4ZSM5 zeolite, the spectrum consists of the same two bands, but the one at 300 nm presents a shift at ~240–260 nm, in addition to the 220 nm band. The addition of TSA leads to an increase in the intensity of the band located at shorter wavelengths and to the appearance of the new ones at 257 and 356 nm, characteristic of the Keggin structure, assigned to $[SiW_{12}O_{40}]^{4-}$ anion [63]. As a result of the increment of TSA content in the samples, there is a red shift of the onset threshold for lower energy, which is highly important for the photoinduced electron transfer processes because it promotes its activity in the visible range. The signal located at 255 nm, assigned to the lacunar species $[SiW_{11}O_{39}]^{8-}$ that could be generated as a result of the decomposition of the anion $[SiW_{12}O_{40}]^{4-}$, was not detected.

The band gap energy (E_g), estimated from DRS-UV–vis spectra using Kubelka–Munk remission function [51], is listed in Table 1. For the zeolites without TSA, the band gap values are in the range 5–6 eV and they are in agreement with those reported in the literature [64]. Zeolite molecular sieves are insulators that cannot be excited even with UV light due to a band gap.

For the NH_4Y and NH_4ZSM5 samples impregnated with TSA, the band gap energy was in the range 3.0–2.9 eV and 3.1–3.0 eV, respectively. These results are similar to those obtained by TPA addition [47].

The morphology and particle size of the materials obtained were analyzed by scanning electron microscopy (Fig. 4). The SEM image of the sample $TSA05NH_4Y$ presents cubic particles and clusters of varying sizes. This morphology is similar to that of NH_4Y zeolite. With increasing content of TSA, the particles, whose morphology is mainly cubic, become both edges rounded vertices. This phenomenon is mainly due to the action of the acidity of the heteropolyacid on the zeolite, together with the thermal treatments to which the samples were subjected during synthesis. For the $TSANH_4ZSM5$ samples, the SEM images present a similar morphology and behavior.

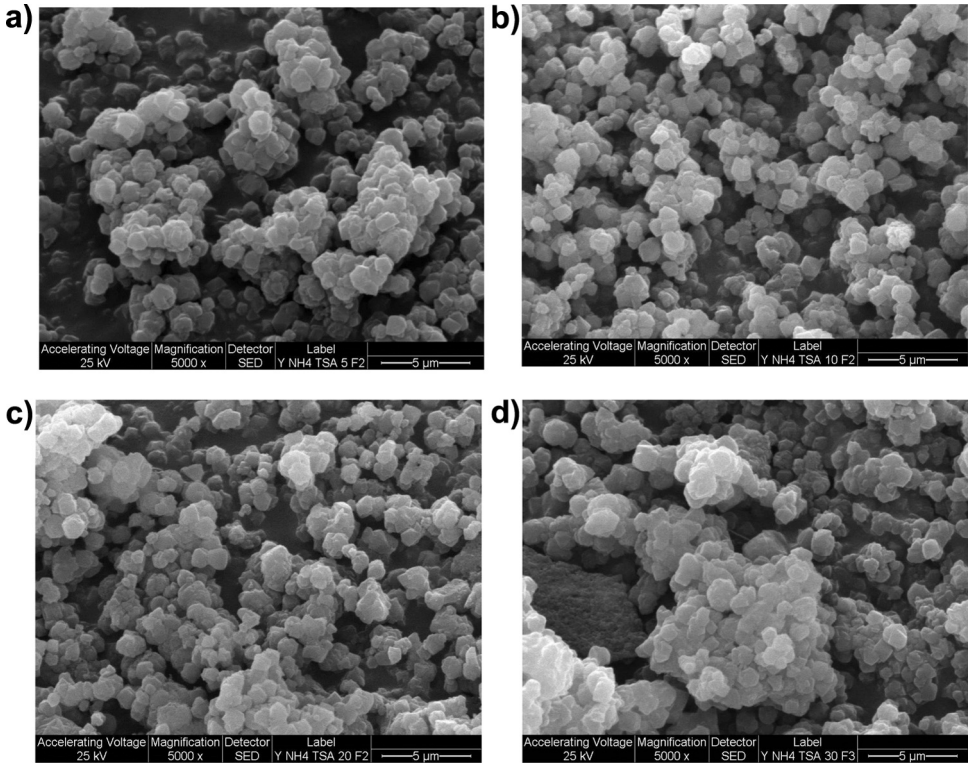

Fig. 4. SEM images of (a) TSA05NH_4Y, (b) TSA10NH_4Y, (c) TSA20NH_4Y and (d) TSA30NH_4Y.

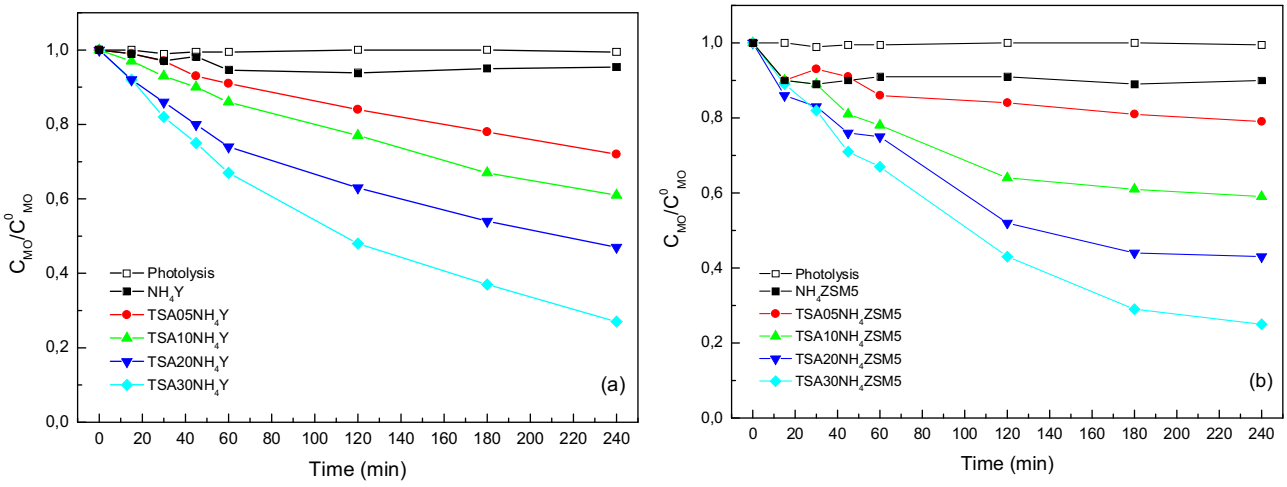

Fig. 5. Photocatalytic degradation of MO as a function of the irradiation time using: a) TSANH_4Y and b) TSANH_4ZSM5 samples. The experimental conditions were: air flow = 0.9 l/min; $C^0_{MO} = 8 \times 10^{-5}$ mol/l; catalyst amount = 200 mg.

3.2. Photocatalytic activity

Fig. 5a and b shows the variation of MO concentration (C_{MO}/C°_{MO}) as a function of time using TSANH_4Y samples and TSANH_4ZSM5 samples as catalysts, respectively. The decrease in the concentration of MO after 240 min of irradiation was only 7% for the NH_4Y sample and it was similar to that achieved for NH_4ZSM5 (10%). Zeolites are insulators that cannot be excited even with UV light ($\lambda < 320$ nm) due to a band gap of about 5–6 eV. We ascribed these values to the absorption of MO molecules on the catalyst surface, although some authors have suggested that the highly isolated Al-O units are the photoactive sites of H-form zeolites or that charge-transfer pairs $[Me^{(n-1)+}\text{-}O^-]^*$ formed upon light excitation ($\lambda < 300$ nm) led to the photocatalytic reactions [65,66]. The amount of MO degraded after 240 min of irradiation without catalyst was only 1%, and it is mainly due to a photolytic process [67].

The increment of the TSA supported on zeolite matrices (NH_4Y and NH_4ZSM5) from 5 to 30%w/w produces a continuous increment of the photocatalytic activity and degradation velocity in the following order: TSA05NH_4Y (28%) < TSA10NH_4Y (39%) < TSA20NH_4Y (53%) < TSA30NH_4Y (73%) and TSA05NH_4ZSM5 (21%) < TSA10NH_4ZSM5 (41%) < TSA20NH_4ZSM5 (57%) < TSA30NH_4ZSM5 (75%), respectively. This behavior is due to the direct participation of TSA in the degradation of the organic substrate. Heteropolyoxometalates (POM) absorb strongly in the near visible and UV region of the light spectrum ($\lambda < 400$ nm), generating a strongly oxidizing excited state POM* (Reaction 1). These species are able to oxidize the

organic substrates (S) (Reaction 2) directly via charge transfer or H-atom abstraction, or indirectly through the intermediacy of solvent-derived radicals [68]. After that process, the corresponding reduced POM is usually reoxidized to its original state by an electron acceptor such as dioxygen (Reaction 3).

$$POM + h\nu \rightarrow POM^{*} \quad (1)$$

$$POM^{*} + S \rightarrow POM^{-} + S^{+} \quad (2)$$

$$POM^{-} + O_2 \rightarrow POM + O_2^{-} \quad (3)$$

The increment in the photocatalytic activity and degradation velocity is also due to the direct participation of TSA in the production of the OH reactive species (Reaction (4)) that participates in the degradation of the organic substrate (Reaction (5)) [69].

$$POM^{*} + H_2O \rightarrow POM^{-} + OH + H^{+} \quad (4)$$

$$OH + S \rightarrow \text{oxidationproducts} \quad (5)$$

Taking into account, from XRD results, that TSA is present in zeolite in the form of $(NH_4)_4[SiW_{12}O_{40}]$ salt, we measured the catalytic activity of the bulk $(NH_4)_4[SiW_{12}O_{40}]$ salt under the same experimental conditions. In this test, the amount of $(NH_4)_4[SiW_{12}O_{40}]$ was fixed in order to obtain a TSA amount similar to that contained in the TSA30-Zeolite samples. MO concentration decreased by 32% at 240 min under reaction and it was lower than those obtained using both TSA30NH_4Y (73%) and TSA30NH_4ZSM5 (75%) samples. According to the results reported by Mizrahi et al. [70] the rather poor catalytic behavior of the $(NH_4)_4[SiW_{12}O_{40}]$ salt could be mainly due to the lower specific surface area of ammonium salt ($101 m^2/g$) in comparison to TSA30-Zeolite samples (Table 1).

3.3. Kinetic study

It has been reported that the photocatalytic degradation of dyes in aqueous systems can be described by pseudo-first-order kinetics with respect to dye concentration [10,71–75] which results from considering that the reaction rate follows the Langmuir–Hinshelwood (L–H) kinetic model:

$$r_{MO} = -\frac{dC_{MO}}{dt} = \frac{k_r K C_{MO}}{1 + K C_{MO}}$$

where r_{MO} is the degradation rate, C_{MO} is the dye concentration, k_r and K are the reaction and adsorption constants, respectively. When C_{MO} is low, KC_{MO} is generally negligible and the reaction rate can be assumed as a pseudo-first-order kinetic with respect to the dye concentration. The resultant equation can be integrated taking into account that C°_{MO} is the dye concentration at time zero, hence,

$$\ln\left(\frac{C^{0}MO}{C}\right) = k_r k\, t$$

From the plots of $\ln(C^{0}_{MO}/C)$ as a function of time, the values of the apparent reaction constant $k_{ap} = k_r K$ were obtained and are shown in Fig. 6.

The values of k_{ap} of the TSANH_4Y and TSANH_4ZSM5 samples in the MO photodegradation increased with a higher TSA content. The increase of k_{ap} is attributed to the direct participation of TSA in the degradation of the organic substrate (Eqs. (1)–(3)) and/or to the direct participation of TSA in the production of the •OH reactive species that participates in the degradation of the organic substrate (Eqs. (4), (5)), as was mentioned.

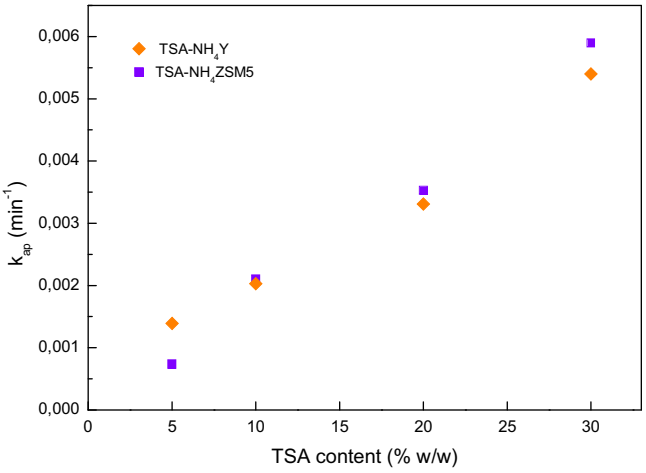

Fig. 6. Values of the apparent reaction constant k_{ap} of the TSANH_4Y and TSANH_4ZSM5 samples at different TSA contents (% w/w).

Generally, first-order kinetics is appropriate for the entire concentration range up to few ppm. It has been reported [76] that the expression for the rate of photomineralization of organic substrates such as dyes with irradiated solid catalysts follows the L–H kinetic model in four possible situations:

(a) The reaction takes place between two adsorbed substances.
(b) The reaction occurs between a radical in solution and an adsorbed substrate molecule.
(c) The reaction takes place between a radical linked to the surface and a substrate molecule in the solution.
(d) The reaction occurs with both species being in the solution.

3.4. Photocatalytic evaluation

In order to study different variables during catalytic evaluation, TSA30NH_4Y was selected. Taking into account that the photodegradation performance was similar for both matrices, the catalyst was selected due to its lower cost since it can be obtained commercially.

The effect of catalyst concentration (C_{CAT}) on the degradation of MO was investigated employing a concentration of TSA30NH_4Y in the range 250–1500 mg/l, keeping all other experimental parameters constant (Fig. 7).

The amount of MO photodegraded at 240 min increased with the increment of C_{CAT} from 0.25 to 0.50 g/l due the availability of active sites on the catalyst surface and the light penetration of photoactivating light into the suspension. The amount of degraded MO increased significantly from 25% to 73% with the increment of C_{CAT} in the above-mentioned range. The amount of photodegraded MO remains practically constant when C_{CAT} increases from 0.50 to 1.0 g/l, and then it decreases for higher C_{CAT} values. This phenomenon was also observed by other authors for the photodegradation of MO, fuchsin acid, malachite green and *p*-nitrophenol [77–79] and it was suggested that an increase in catalyst concentration, will provide more reactive sites, resulting in the enhancement of the decolorization rate. At a higher level of catalyst concentration, although the reactive sites increased the solution became cloudy and opaque, which reduced light penetration. As a result, part of the catalyst surface became unavailable for photon absorption and the decolorization rate decreased.

The possibility to easily recover and reuse the materials obtained in this investigation was evaluated. For this purpose after each reaction, the catalyst was recovered by filtration, washed with distilled

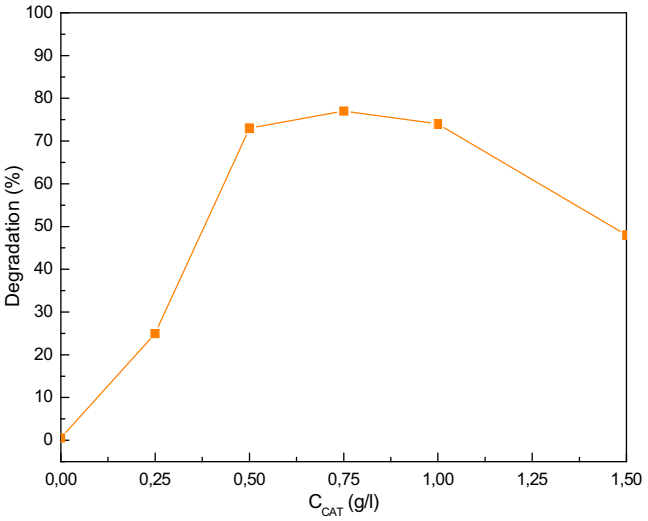

Fig. 7. Effect of TSA30NH_4Y catalyst amount on MO degradation.

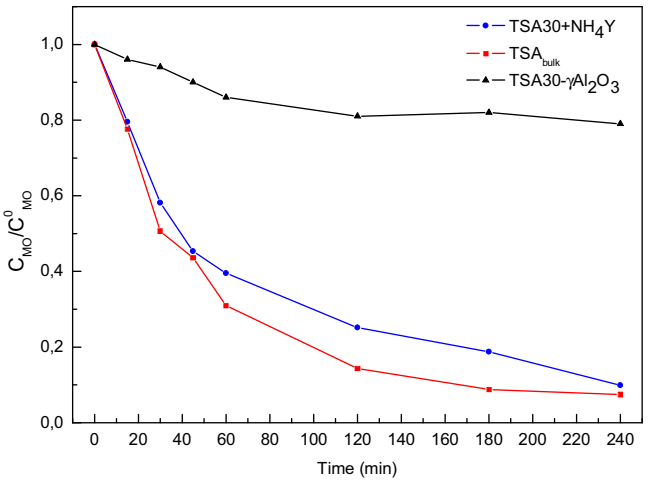

Fig. 8. Comparative photocatalytic activity of TSA_{bulk}, TSA30 + NH_4Y (physical mixture) and TSA30-γAl_2O_3.

water, dried at 70 °C, and then reused without any calcination treatment. The MO degradation obtained after the first cycle of reuse was significantly lower (36%) than that obtained using the fresh catalyst (73%). A similar behavior was reported by Subba Rao et al. [80]. Ökte and Yilmaz [81] and Zhu et al. [82]. They claimed that the decline in the catalyst activity after a certain number of reuses could be due to the adsorption of the reaction products on the catalyst surface and the photocatalyst active sites, which render them unavailable for decolorization of fresh dye solution. Adsorbed products can be removed by an adequate thermal treatment. However, this treatment could induce the sintering of catalyst particles and structural changes that could also reduce the photocatalytic activity.

In order to study this possibility, after the first reuse the catalyst was separated by filtration, treated at 200 °C for 2 h, and reused again. Although the MO degradation value using the catalyst treated in this way increased (59%), the activity was not completely restored. The XRD pattern of TSA30NH_4Y calcined at 200 °C present similar features to those of the fresh one with no considerable reduction in crystallinity. However, it is not possible to exclude the sintering of the catalyst particles. The main reason for the slightly smaller photocatalytic activity of the calcined sample could be because the calcination temperature applied to the material was not enough to completely remove the remaining adsorbed molecules on the catalyst surface and therefore, the photocatalytic activity decreases, as was corroborated in the FT-IR spectra.

Polyoxometalates can be used as bulk or supported catalysts owing to special properties. However, one of the major drawbacks of bulk polyoxometalates is related to their high solubility in oxygenated solvents (such as water) thus make impossible its subsequent recovery and reuse. For comparison purposes, we evaluated the catalytic activity of bulk TSA as homogeneous catalyst. In this test, the TSA amount was fixed in order to obtain a tungstosilicic acid amount similar to that contained in the TSA30NH_4Y sample. Under those conditions (homogeneous reaction due to the complete TSA dissolution in the aqueous media), MO was practically degraded at 180 min (Fig. 8). However the TSA catalyst cannot be recovered and reused. We also evaluated a physical mixture of TSA and NH_4Y zeolite (TSA30 + NH_4Y) with a TSA content similar to that contained in the TSA30NH_4Y sample (Fig. 8). MO concentration decreased by 91% at 240 min under reaction and it was similar to that obtained with bulk TSA. After the photocatalytic experiment, the catalysts was separated from the solution, dried at 70 °C and reused. No significant MO degradation was detected. This was attributed to the complete TSA solubilisation in the MO water solution and it was confirmed by atomic absorption spectrometry. Additionally, the catalytic activity of TSA supported (30% w/w in the final solid) on γ-Al_2O_3 (surface area 280 m^2/g; mean pore diameter 3.4 nm) was evaluated [32]. After 240 min under irradiation, the MO concentration decreased only 21%. The rather poor catalytic activity was attributed to the transformation of TSA into the lacunary specie $[SiW_{11}O_{39}]^{8-}$. When an alkali material was used as support, a complex series of reactions takes place leading to different lacunar species. The Keggin anion of TSA finally decomposes into $[SiO_3]^{2-}$ and $[WO_4]^{2-}$ via the species $[SiW_{11}O_{39}]^{8-}$ and $[SiW_9O_{34}]^{10-}$ [83]. So, we can conclude that γ-Al_2O_3 is not suitable as TSA support.

The solution pH is an important variable in aqueous phase mediated photocatalytic reactions. The solution pH influences the adsorption and dissociation of the substrate, the catalyst surface charge, and other physicochemical properties of the systems [84]. The effect of pH on the photocatalytic degradation of MO by TSA30NH_4Y was studied. The experiments were performed at acidic (pH 2.5) and alkaline (pH 11) pH values of the MO solution, keeping all other experimental conditions constant. The amount of degraded MO slightly increased at pH 2.5 (from 73% to 85%) at the same irradiation time (240 min) and it considerably decreased (from 73% to 28%) at pH 11. A similar influence of the pH on the photodegradation of MO was reported when employing solar light or UV light sources with TiO_2 as catalyst in FBR or batch reactors [7,77,85]. The effect of pH on the photocatalytic reactions is generally attributed to the surface charge of solids and its relation to the ionic form of the organic compound (anionic or cationic). At higher pH than the point of zero charge (p_{zc}) of the catalyst, the surface is negatively charged. At pH > p_{zc}, the MO due to the negatively charged group is repelled by the surface of the catalyst negative charge reducing the possibility of adsorption and hence, the photodegradation decreases.

4. Conclusion

Catalysts based on TSA supported on NH_4Y and NH_4ZSM-5 zeolites were synthesized successfully by wet impregnation. The results of characterization techniques revealed that the surface area of the materials decreased when a higher amount of TSA was added due to pore entrance blocking by the anion $[SiW_{12}O_{40}]^{4-}$ in both matrices. XRD patterns indicate that TSA was incorporated in the form of the cubic salt $(NH_4)_4[SiW_{12}O_{40}]$, whose generation was a result of the interaction of the anion $[SiW_{12}O_{40}]^{4-}$ with the cations $[NH_4]^+$ of zeolites. The results of DRS-UV–vis of the samples display an absorption threshold onset that continuously shifts to the

visible region with the increment of TSA content. The E_g values of TSA-Zeolite samples were similar to those reported for TiO_2.

According to photocatalytic activity results, the increment in the amount of TSA supported on the zeolite matrices caused a continuous increase in photocatalytic activity and degradation velocity, due to the direct participation of TSA in the degradation of the organic substrate and/or in the production of the OH reactive species. The photocatalytic degradation of MO was described by pseudo-first-order kinetics with respect to dye concentration. The values of k_{ap} of the $TSANH_4Y$ and $TSANH_4ZSM5$ samples increased with higher TSA content, which is attributed to the direct participation of TSA in the photodegradation process. The optimum catalyst concentration was 0.5 g/l, and an increase in the catalyst amount decreased the degradation rate because the solution became cloudy and opaque, reducing light penetration. The effect of pH on the photocatalytic degradation was studied by varying the initial pH of the MO solution and keeping all other experimental conditions constant. A decrease in pH changed the surface state of the catalyst and increased MO adsorption, which is beneficial to the photocatalytic rate.

The effect of supported TSA on zeolites generated recoverable and reusable materials with an increased surface area. The materials obtained presented suitable properties to be used as catalysts in the photocatalytic treatment of wastewater that containing dyes.

References

[1] T. Robinson, G. McMullan, R. Marchant, P. Nigam, Bioresour. Technol. 77 (2001) 247–255.
[2] D. Melgoza, A. Hernandez-Ramirez, J.M. Peralta-Hernandez, Photochem. Photobiol. Sci. 8 (2009) 596–599.
[3] T. Phani Madhavi, M. Srimurali, K. Nagendra Prasad, J. Environ. Res. Dev. 8 (2014) 890–894.
[4] L. Pereira, R. Pereira, M.F.R. Pereira, F.P. VanderZee, F.J. Cervantes, M.M. Alves, Hazard. Mater. 183 (2010) 931–939.
[5] Advanced Oxidation Technologies, Sustainable Solutions for Environmental Treatments, in: M. Litter, R.J. Candal, J.M. Meichtry (Eds.), CRC Press, Netherlands, 2014.
[6] J.M. Herrmann, C. Guillard, P. Pichat, Catal. Today 17 (1993) 7–20.
[7] S. Al-Qaradawi, S.R. Salman, J. Photochem. Photobiol. A: Chem. 148 (2002) 161–168.
[8] R. Wakimoto, T. Kitamura, F. Ito, H. Usami, H. Moriwaki, Appl. Catal. B: Environ. 166–167 (2015) 544–550.
[9] L.C. Chen, T.C. Chou, Ind. Eng. Chem. Res. 33 (6) (1994) 1436–1443.
[10] Y. Li, X. Li, J. Li, J. Yin, Water Res. 40 (2006) 1119–1126.
[11] X.H. Wang, J.G. Li, H. Kamiyama, Y. Moriyoshi, T. Ishigaki, J. Phys. Chem. B 110 (13) (2006) 6804–6809.
[12] V. Augugliaro, C. Baiocchi, A. Bianco Prevot, E. García-López, V. Loddo, S. Malato, G. Marcí, L. Palmisano, M. Pazzi, E. Pramauro, Chemosphere 49 (2002) 1223–1230.
[13] I.V. Kozhevnikov, J. Mol. Catal. A: Chem. 262 (2007) 86–92.
[14] Z. Hou, T. Okuhara, Chem. Commun. (2001) 1686–1687.
[15] N. Lingaiah, N. Babu, K. Reddy, P. Prasad, I. Suryanarayana, Chem. Commun. (2007) 278–279.
[16] M. Yoon, J. Chang, Y. Kim, J. Choi, J. Phys. Chem. B 105 (2001) 2539–2545.
[17] H. Hori, Y. Takano, K. Koike, K. Takeuchi, H. Einaga, Environ. Sci. Technol. 37 (2003) 418–422.
[18] A. Corma, H. García, F.X.L. Xamena, Chem. Rev. 110 (2010) 4606–4655.
[19] B. Sulikowski, R. Rachwalik, Appl. Catal. A: Gen. 256 (2003) 173–182.
[20] L.R. Pizzio, M.N. Blanco, Appl. Catal. A: Gen. 255 (2003) 255–265.
[21] J.S. Santos, J.A. Dias, S.C.L. Dias, F.A.C. Garcia, J.L. Macedo, F.S.G. Sousa, L.S. Almeida, Appl. Catal. A: Gen. 394 (2011) 138–148.
[22] A. Hiskia, A. Mylonas, E. Papaconstantinou, Chem. Soc. Rev. 30 (2001) 62–69.
[23] P. Kormali, A. Troupis, T. Triantis, A. Hiskia, E. Papaconstantinou, Catal. Today 124 (2007) 149–155.
[24] J.H. Choi, T.H. Kang, J.H. Song, Y. Bang, I.K. Song, Catal. Commun. 43 (2014) 155–158.
[25] K. Pruethiarenun, T. Isobe, S. Matsushita, J. Ye, A. Nakajima, Mater. Chem. Phys. 144 (2014) 327–334.
[26] R.R. Ozer, J.L. Ferry, J. Phys. Chem. B 106 (2002) 4336–4342.
[27] I.V. Kozhevnikov, Chem. Rev. 98 (1998) 171–198.
[28] Y. Chen, Y. Cao, Y. Suo, G.P. Zheng, X.X. Guan, X.C. Zheng, J. Taiwan Inst. Chem. Eng. (2015) 1–7.
[29] K. Pamin, A. Kubacka, Z. Olejniczak, J. Haber, B. Sulikowski, Appl. Catal. A: Gen. 194–195 (2000) 137–146.
[30] Y. Guo, Y. Wang, C. Hu, Y. Wang, E. Wang, Chem. Mater. 15 (2000) 3501–3508.
[31] S.R. Mukai, L. Lin, T. Masuda, K. Hashimoto, Chem. Eng. Sci. 56 (2001) 799–804.
[32] L.R. Pizzio, C. Cáceres, M. Blanco, Appl. Catal. A: Gen. 167 (1998) 283–294.
[33] M.V. Phanikrishna Sharma, V. Durgakumari, M. Subrahmanyam, J. Hazard. Mater. 160 (2008) 568–575.
[34] P.K. Dutta, Y. Kim, Curr. Opin Solid State Mater. Sci. 7 (2003) 483–490.
[35] H. Chen, A. Matsumoto, N. Nishimiya, K. Tsutsumi, Colloids Surf. A: Physicochem. Eng. Aspects 157 (1999) 295–305.
[36] Y. Kim, M. Yoon, J. Mol. Catal. A: Chem. 168 (2001) 257–263.
[37] P.K. Dutta, W. Turbeville, J. Phys. Chem. 96 (1992) 9410–9416.
[38] X. Liu, K. Kong Iu, J.K. Thomas, J. Chem. Soc. Faraday Trans. 89 (1993) 1861–1865.
[39] A.G. Panov, R.G. Larsen, N.I. Totah, S.C. Larsen, V.H. Grassian, J. Phys. Chem. B 104 (2000) 5706–5714.
[40] H. Sun, F. Blatter, H. Frei, J. Am. Chem. Soc. 116 (1994) 7951–7952.
[41] H. Sun, F. Blatter, H. Frei, J. Am. Chem. Soc. 118 (1996) 6873–6879.
[42] S. Uppili, K.J. Thomas, E.M. Crompton, V. Ramamurthy, Langmuir 16 (2000) 265–274.
[43] K.B. Yoon, Chem. Rev. 93 (1993) 321–339.
[44] L. Yang, K. Trafford, O. Kresnawahjuesa, J. Sepa, R.J. Gorte, D. White, J. Phys. Chem. B 105 (2001) 1935–1942.
[45] P.K. Dutta, J.A. Injavo, J. Phys. Chem. 91 (1987) 4443–4446.
[46] V. Ramamurthy, P. Lakshminarasimhan, C.P. Grey, L.J. Johnston, Chem. Commun. 22 (1998) 2411–2424.
[47] C. Leal Marchena, R.A. Frenzel, S. Gomez, L.B. Pierella, L.R. Pizzio, Appl. Catal. B: Environ. 130–131 (2013) 187–196.
[48] L. Chen, X. Wang, X. Guo, H. Guo, H. Liu, Y. Chen, Chem. Eng. Sci. 62 (2007) 4469–4478.
[49] P. Chu, US Patent No. 3.709. 979, 1972.
[50] T. Ito, K. Inumaru, M. Misono, J. Phys. Chem. B 101 (1997) 9958–9963.
[51] W.W. Wendlant, H.G. Hecht, Reflectance Spectroscopy, Wiley, New York, 1966.
[52] M. Rochkind, S. Pasternak, Y. Paz, Molecules 20 (2015) 88–110.
[53] P. Morales-Pacheco, J.M. Domínguez, L. Bucio, F. Álvarez, U. Sedrán, M. Falco, Catal. Today 166 (2011) 25–38.
[54] C. Rocchiccioli-Deltcheff, R. Thouvenot, R. Franck, Spectrochim. Acta A 32 (1976) 587–597.
[55] I. Othman, R.M. Mohamed, I.A. Ibrahim, M. Mokhtar Mohamed, Appl. Catal. A: Gen. 299 (2006) 95–102.
[56] L. Pizzio, M. Blanco, Microporous Mesoporous Mater. 103 (2007) 40–47.
[57] J.B. Mioc, R.Z. Dimitrijevi, M. Davidovic, Z.P. Nedic, M.M. Mitrovic, P.H. Colomban, J. Mater. Sci. 29 (1994) 3705–3718.
[58] F. Lefebvre, J. Chem. Soc. Chem. Commun. (1992) 756–757.
[59] L. Pizzio, P. Vázquez, A. Kikot, E. Basaldella, C. Cáceres, M. Blanco, Stud. Surf. Sci. Catal. 143 (2002) 739–746.
[60] M. Hasik, W. Turek, E. Stochmal, M. Lapkowski, A. Pron, J. Catal. 147 (1994) 544–551.
[61] P. Vázquez, L. Pizzio, C. Cáceres, M. Blanco, H. Thomas, E. Alesso, L. Finkielsztein, B. Lantaño, G. Moltrasio, J. Aguirre, J. Mol. Catal. A: Chem. 161 (2000) 223–232.
[62] M.A. Zanjanchi, A. Razavi, Spectrochim. Acta A 57 (2001) 119–127.
[63] K. Nomiya, Y. Sugie, K. Amimoto, M. Miwa, Polyhedron 6 (1987) 519–524.
[64] G. Yan, J. Long, X. Wang, Z. Li, X. Fu, CR Chimie 11 (2008) 114–119.
[65] M. Anpo, M. Matsuoka, Y. Shioya, H. Yamashita, J. Phys. Chem. 98 (1994) 5744–5750.
[66] Y. Kato, H. Yoshida, A. Satsuma, T. Hattori, Microporous Mesoporous Mater. 51 (2002) 223–231.
[67] M.A. Barakat, H. Schaeffer, G. Hayes, S. Ismat-Shah, Appl. Catal. B: Environ. 57 (2005) 23–30.
[68] R.R. Ozer, J.L. Ferry, J. Phys. Chem. B 104 (2000) 9444–9448.
[69] S. Antonaraki, T.M. Triantis, E. Papaconstantinou, A. Hiskia, Catal. Today 151 (2010) 119–124.
[70] D.M. Mizrahi, S. Saphier, I. Columbus, J. Hazard. Mater. 179 (2010) 495–499.
[71] H. Lachheb, E. Puzenat, A. Houas, M. Ksibi, E. Elaloui, C. Guillard, J.M. Herrmann, Appl. Catal. B 39 (2002) 75–90.
[72] K. Tanaka, K. Padermpole, T. Hisanaga, Water Res. 34 (2000) 327–333.
[73] V. Fuchs, L. Méndez, M. Blanco, L. Pizzio, Appl. Catal. A: Gen. 358 (2009) 73–78.
[74] H.J. Lee, J.H. Kim, S.S. Park, S.S. Hong, G.D. Lee, J. Ind. Eng. Chem. 25 (2015) 199–206.
[75] I.K. Konstantinou, T.A. Albanis, Appl. Catal. B: Environ. 49 (2004) 1–14.
[76] M.N. Rashed, A.A. El-Amin, Int. J. Phys. Sci. 2 (2007) 73–81.
[77] W. Nam, J. Kim, G. Han, Chemosphere 47 (2002) 1019–1024.
[78] J.H. Lee, W. Nam, M. Kang, G.Y. Han, K.J. Yoon, M.S. Kim, K. Ogino, S. Miyata, S.J. Choung, Appl. Catal. A: Gen. 244 (2003) 49–57.
[79] K. Zhao, Y. Lu, N. Lu, Y. Zhao, X. Yuan, H. Zhang, L. Teng, F. Li, Appl. Surf. Sci. 285 (2013) 616–624.
[80] K.V. Subba Rao, M. Subrahmanyam, P. Boule, Appl. Catal. B: Environ. 49 (2004) 239–249.
[81] A.N. Ökte, Ö. Yilmaz, Appl. Catal. A: Gen. 354 (2009) 132–142.
[82] H. Zhu, R. Jiang, Y. Fu, Y. Guan, J. Yao, L. Xiao, G. Zeng, Desalination 286 (2012) 41–48.
[83] L.R. Pizzio, C.V. Cáceres, M.N. Blanco, J. Colloid Interface Sci. 190 (1997) 318–326.
[84] M. Mahalakshmi, S. Vishnu Priya, B. Arabindoo, M. Palanichamy, V. Murugesan, J. Hazard. Mater. 161 (2009) 336–343.
[85] L.C. Chen, F.R. Tsai, C.M. Huang, J. Photochem. Photobiol. A 170 (2005) 7–14.